# Molecular dynamics study of mechanical properties of carbon nanotube-embedded gold composites

Song HaiYang*, Zha XinWei

(Department of Applied Mathematics and Applied Physics, Xi'an Institute of Posts and Telecommunications, Xi'an 710121, P R China)

**Abstract**

The mechanical properties of nano-single crystal gold carbon nanotube-embedded gold (CNT/Au) composites under axial tension were investigated using molecular dynamics (MD) simulation method. The interactions between atoms were modeled using the many-body tight-binding (TB) potential and the empirical Tersoff potential coupled with the Lennard-Jones (L-J) potential. We get the yield strain and the yield stress of nano-single crystal gold 0.092, 5.74 GPa, respectively. The computational results show that the increase in Young's modulus of the long CNT-embedded gold composite over pure gold is much large. From the simulation, we also find that the yield stress and the yield strain of short CNT-embedded gold composite are evidently less than that of the nano-single crystal gold.

*Key words:* molecular dynamics simulation; carbon nanotubes; carbon nanotube-embedded gold composites

PACS number: 61.48. +c; 81.05.Ni; 62.25.+g

## 1. Introduction

Since the first report of CNT by Iijima [1], research on CNTs has been attracting much attention to explore their unusual electronic and mechanical properties. Both theoretical and

*Corresponding Author. Department of Applied Mathematics and Applied Physics, Xi'an Institute of Posts and Telecommunications, Xi'an 710121, PR China. Tel: +86-029-88166094.
*E-mail address:* gsfshy@sohu.com (S. HaiYang)

experimental studies indicated that CNTs are material with extraordinary high stiffness and axial strength [2-15]. These outstanding mechanical characteristics combined with their extremely high strength to weight ratio make them potential candidates as reinforcing fibers in super strong composites. R. Zhu et al. [16] have used molecular dynamic to evaluate the stress-strain behavior of CNT-reinforced Epon 862 composites. Their simulation results show that the long CNT-reinforced Epon 826 composite can be at least 10 times stiffer than the pure Epon 862 matrix. Even for the short CNT-reinforced Epon 862 composite, its effective Young's modulus can be also increased by roughly 20% as compared to the Epon 862 matrix. D. Qian et al. [17] also have demonstrated that the stiffness of the composite film with 1% (by weight) CNTs can been increased by up to 42% and the tensile strength by 25%. At present, there has been more interest in using metal as the matrix material for composites [18,19]. It has been found that the fracture toughness of a metal matrix composite with CNTs can be increased by up to 200% [19].

In this paper, we investigate the mechanical properties of three models, namely, a long CNT-embedded gold composites, a short CNT-embedded gold composites and nano-single crystal gold itself, under uniaxial tension using MD simulation method. From our simulations, we obtain the yield strain and the yield stress of nano-single crystal gold. Some new findings from this study are also reported.

This paper is organized in the following way. In Sec.II we describe the inter-atomic potentials for MD simulation. Sec.III provides the simulation model. Results and discussion are given in Sec.IV. The final section is the conclusions.

## 2. The inter-atomic potential function

The use of inter-atomic potentials to model the energetic and dynamics of nano-scale

structures lies at the very foundation of the computer-based MD simulations. The MD simulation is the powerful tool for investigation of the mechanical properties of nanocomposite. The selection of potential function is a key factor, which determinates the result's accuracy in MD simulation. In this work, the many-body TB potential [20] is used for modeling the gold-gold interaction, the Tersoff potential [21] for the carbon-carbon interaction, while the gold-CNT interaction is modeled with a L-J potential [22]. The expression for the total energy of the CNT-Au composite system is written as:

$$E_{tatol} = E_{CNT} + E_{Au} + E_{LJ} \tag{1}$$

where $E_{tatol}$ is the total potential energy of the CNT-Au composite, $E_{CNT}$ and $E_{Au}$ are the potential of CNT and Au matrix, respectively. $E_{LJ}$ is the energy of interaction between the CNT and the gold matrix. The models for these components are described next.

**2.1. Potential model for Au matrix**

The gold systems are modeled using the many-body TB potential. The prediction of some characteristics by the TB potential has been proven to be more accurate than that of the EAM method for some transition metals. For the gold system the total energy can be expression as:

$$E_{Au} = -\sum_i \left[ \sum_{j \neq i} \xi^2 \exp[-2q\left(\frac{r_{ij}}{r_0} - 1\right)] \right]^{1/2} + \sum_i \sum_{j \neq i} A \exp[-p\left(\frac{r_{ij}}{r_0} - 1\right)] \tag{2}$$

where $r_{ij}$ represents the distance between atoms $i$ and $j$, $\xi$ and $r_0$ are respectively an effective hopping integral and the nearest neighbor distance in the gold lattice. The parameter $q$, $p$ and $A$ are adjustable parameters depending on the interacting atomic species. In Eq. (2), the first potential term is a many body term as obtained by the tight binding second-moment model, and the second term, arising from the interaction of the electronic densities localized on the atomic nuclei, is a simple sum of pair wise repulsion terms. The detailed information and parameters of

Eq. (2) are given in Cleri's paper [20].

### 2.2. Potential model for CNT/Au composites

The empirical bond order potential proposed by Tersoff is employed to describe interatomic interation in CNT. This Tersoff potential can be formally written as a summation of pairwise interactions,

$$E_{CNT} = \sum_{i>j} f_c(r_{ij})[V_R(r_{ij}) - b_{ij}V_A(r_{ij})], \tag{3}$$

where the function $V_R(r_{ij})$ represents the repulsive part-wise of the potential, such as the core-core interactions, and the function $V_A(r_{ij})$ represents the bonding due to the valence electrons, and their functional forms are given as:

$$V_R(r) = A_{ij}\exp(-\lambda r) \quad , \quad V_A(r) = B_{ij}\exp(-\mu r) \tag{4}$$

$$f_c(r) = \begin{cases} 1, & r < R_{ij}, \\ \frac{1}{2}\left[1 + \cos\frac{\pi(r - R_{ij})}{S_{ij} - R_{ij}}\right], & R_{ij} \le r \le S_{ij}, \\ 0 & r > S_{ij}, \end{cases} \tag{5}$$

where $f_c(r)$ is a cutoff function, which explicitly restricts the interactions within the nearest neighbors and dramatically reduces the redundant computation in the force potential evaluation procedure. In Eq. (3), $b_{ij}$ is a bond order parameter and depends on the bonding environment around atoms $i$ and $j$. $b_{ij}$ implicitly contains many-body information and thus the whole potential functions is actually a multiple-body potential. The functional form of $b_{ij}$ can be written as follows:

$$b_{ij} = [1 + (\beta_i \xi_{ij})^{n_i}]^{-1/2n_i} \tag{6}$$

The (weak) nonbonded interactions between gold atoms and carbon atoms are modeled with a simple LJ potential.

$$E_{ij}^{LJ} = 4\varepsilon\left[-\left(\frac{\sigma}{r_{ij}}\right)^{6} + \left(\frac{\sigma}{r_{ij}}\right)^{12}\right], \tag{7}$$

where $\varepsilon$ and $\sigma$ are the coefficients of well-depth energyand and the equilibrium distance, respectively. The parameters for the interactions between carbon atoms and gold atoms are given in [22] ($\varepsilon_{C-Au} = 0.01272eV$, $\sigma_{C-Au} = 0.29943nm$).

## 3. Simulation model

The initial atomic configuration of nano-single crystal gold is arranged with the ideal lattice as shown in Fig. 1a, and the models of the long CNT/Au composites and the short CNT/Au are shown in Fig. 1b and Fig. 1c, respectively. The crystal orientation was [100, 010, 001]. To simulate uniaxial tension, the prescribed displacement is applied along the $z$-direction, namely, the axial direction of the CNT. All models have equal dimension: length of 2.45nm, width of 2.45nm, and depth of 5.3nm. A long (4, 4) armchair CNT and a short (4, 4) CNT, which have length of 5.3nm and 2.65nm, are embedded in the gold matrix, respectively. The simulation process includes the following steps: relaxing the initial configuration to reach the equilibrium state, fixing boundary condition at one end of the tube, applying the tension along the axial direction at another rigid end by external displacement, then relaxing the system to reach a new equilibrium state and a new configuration.

All models have a strain of 0.001 along the axis in each step, and the whole model is fully relaxed while keeping the two ends constrained. Each relaxation time is 4.5 $ps$, and the whole simulation process includes 1500 steps. The environmental temperature keeps 0.01K to avoid the thermal kinetic effect.

## 4. Results and discussion

A MD simulation is performed to obtain the minimum energy state of the systems without any applied deformation. The simulation is performed approximately 30.0 ps with a time step of 3.0 fs for all models, after which the energy attains the constant minimum value. Fig. 2 shows the total potential energy variation in the equilibration process of crystal gold. As shown in Fig. 2, the system is stable after 3000 molecular dynamics steps. The inset of Fig. 2 is the curve of approach equilibrium. It can be seen that the total potential energy fluctuates about a steady value after the system attains the equilibrium state.

## 4.1 Mechanical properties of crystal gold

We first investigate the mechanical behavior of the nano-single crystal gold under uniaxial tension using our molecular dynamics simulation program. By definition the stress $\sigma$ is given by $\sigma = F/A$, where $A$ stands for the area of the cross section of the crystal. $F$ is the force of maintaining the constraint on the system, which can be obtained by summing the interatomic force for the atoms at the end of the crystal. Fig. 3 shows the stress-strain curves based on stress $\sigma$, measured in the $z$-direction, and longitudinal strain $\varepsilon$. The deformation is elastic in the initial stage of tensile deformation of crystal gold. The Young's modulus is evaluated as the slope of stress-strain curve at initial tangent. Based on the above method, we obtain the Young's modulus of the nano-single crystal gold 66.22 GPa. It can be also seen that there exists a maximum value of stress, which is called yield stress. Corresponding strain is called yield strain. The maximum stress is 5.74 GPa at strain of 0.092. Upon reaching the yield strain, the stress decreases suddenly and the tensile deformation is in the flow of plasticity. The yield stress of 5.74 Gpa and the Young's modulus of 66.22 GPa, obtained from the stress-strain curve, are in good agreement with the existing experimental results [23].

To visualize the process of tensile deformation of nano-single crystal gold, the stress-strain curve's corresponding atomic arrangements are shown in Fig. 4. After relaxation, the initial set-up of the crystal is shown in Fig. 4(a). When the crystal stretches to yield strain of 0.092, the deformation of nano-single crystal gold still is elastic as shown in Fig. 4(b). Upon reaching the yield strain, the crystal structure experienced an abrupt dislocation, as displayed in Fig. 4(c). With the strain increasing, the dislocations continue to occur and move, propagate, and slips take place as shown in Fig. 4(d). From Fig. 4(d), it can be clearly seen that slippage occurred along the (111) plane. As explained by S.J.A. Koh [24], the reason for this is that the smallest Burgers vector existing in the [110] close-packed directions for fcc crystal structures, making it most energetically favorable to reconstruct along this plane.

## 4.2 Mechanical properties of CNT/Au composites

Now we examine the mechanical behaviors of long CNT-embedded gold composite and short CNT-embedded gold composite. The results are characterized by the relationship of stress $\sigma$ and strain $\varepsilon$. Fig. 5 shows the stress-strain curves for the nano-single crystal gold, the long CNT-embedded gold composite and the short CNT-embedded gold composite under uniaxial tension. As expected, the increase in Young's modulus of the long CNT-embedded gold composite over pure gold is much large. This is evident from the fact that the modulus of 1009.1 Gpa for the armchair (4, 4) CNT is about fifteen times that of 66.22GPa for the nano-single crystal gold. It is observed form Fig. 5 that the short CNT could also improve the corresponding composite stiffness although not as significant as that in the long CNT-embedded composite. Unfortunately, the yield stress and the yield strain of short CNT-embedded gold composite are evidently less than that of the pure nano-single crystal gold. The reason for this is that the interaction between CNT and

nano-single crystal gold is too weak for effective load transfer. The short, embedded CNT may act like a void, reducing the yield stress and the yield strain. The equilibrium structure and the structure at 0.04 strain of the short CNT-embedded gold composite are shown in Fig. 6(a) and (b), respectively. It can be clearly seen that the dislocations of the composite appear in one end of embedded CNT. The result is completely consistent with our physical interpretations mentioned above.

## 5. Conclusions

Using MD method, we investigate in detail the mechanical behaviors of the nano-single crystal gold, the long CNT-embedded gold composite and the short CNT-embedded gold composite under uniaxial tension. The results show that the yield stress 5.74 GPa and the Young's modulus 66.22 GPa of nano-single crystal gold are very closed to the existing experimental results. As expected, the increase in stiffness of the long CNT-embedded gold composite over the pure nano-single crystal gold matrix is much large. We also obtain the yield stress and the yield strain of the short CNT-embedded gold composite, and find that they are evidently less than that of the nano-single crystal gold. But the stiffness of the short CNT-embedded gold composite is lightly bigger than that of pure gold matrix.

## Acknowledgements

This work is supported by the Shaanxi Natural Science Foundation (Grant No.2004A15) and Science Plan Foundation of office the Education Department of Shaanxi Province (Grant No. 05JK288).

## References

[1] S. Iijima, Nature 354 (1991) 56.

[2] B.I. Yakobson, C.J. Brabec, J. Bernholc, Phys. Rev. Lett. 76 (1996) 2511.

[3] J. Cai, R.f. Bie, X.M. Tan et al, Physica B 344 (2004) 99.

[4] H.Y. Song, H.M. Sun, G.X. Zhang, Commun. Theor. Phys. 45 (2006) 741.

[5] C.L. Zhang, H.S. Shen, Carbon 44 (2006) 2608.

[6] Y. Jin and F.G. Yuan, Compos. Sci. Technol. 63 (2003) 1507.

[7] W.X. Bao, C.C. Zhu, W.Z. Cui, Physica B 352 (2004) 156.

[8] H.Y. Song, X.W. Zha, Physica B 393 (2007) 217.

[9] A. Krishnan, E. Dujardink, T.W. Ebbesen, Phys. Rev. B 58 (1998) 14013.

[10] H.S. Shen, C.L. Zhang, Phys. Rev. B 74 (2006) 035410.

[11] K.M. Liew, X.Q. He, C.H. Wong, Acta. Mater. 52 (2004) 2521.

[12] K.M. Liew, C.H. Wong, X.Q. He, et al., Phys. Rev. B 69 (2004) 115429.

[13] S.H. Yeak, T.Y. Ng, K.M. Liew, Phys. Rev. B 72 (2005) 165401.

[14] K.M. Liew, C.H. Wong, M.J. Tan, Acta. Mater. 54 (2006) 225.

[15] G.X. Gao, X. Chen, Phys. Rev. B 73 (2006) 155435.

[16] R. Zhu, E. Pan, A.K. Roy, Mater. Sci. Eng. A 447 (2007) 51.

[17] D. Qian, E.C. Dickey, R. Andrews, et al., Appl. Phys. Lett. 76 (2000) 2868.

[18] S.P. Xiao, W.Y. Hou, Phys. Rev. B 73 (2006) 115406.

[19] T. Kuzumaki, K. Miyazawa, H. Ichinose, et al., J. Mater. Res. 13 (1998) 2445.

[20] F. Cleri, V. Rosato, Phys. Rev. B 48 (1993) 22.

[21] J. Tersoff, Phys. Rev. B 39 (1989) 5566.

[22] S. Arcidiacono, J.H. Walther, D. Poulikakos, et al., Phys. Rev. Lett. 94 (2005) 105502.

[23] J.D. Kiely, J.E. Houston, Phys. Rev. B 57 (1998) 12588.

[24] S.J.A. Koh, H.P. Lee, C. Lu, et al., Phys. Rev. B 72 (2005) 085414.

# Figure Captions

**Fig. 1** The atomic structure of (a) crystal gold, (b) long CNT/Au composites and (c) short CNT/Au composites.

**Fig. 2** Total potential energy variation in equilibration process of crystal gold. The inset is the curve of approach equilibrium.

**Fig. 3** The curves of variation of stress $\sigma$ with strain $\varepsilon$ (crystal gold).

**Fig. 4** Snapshots of atomic arrangement of crystal gold at various strain values. (a) $\varepsilon = 0.000$, (b) $\varepsilon = 0.092$, (c) $\varepsilon = 0.095$, (d) $\varepsilon = 0.300$.

**Fig. 5** The curves of variation of stress $\sigma$ with strain $\varepsilon$ (crystal gold, long CNT-embedded gold composites and short CNT-embedded gold composites).

**Fig. 6** Snapshots of atomic arrangement of short CNT-embedded gold composites at various strain values. (a) $\varepsilon = 0.000$, (b) $\varepsilon = 0.400$.

**Potential Reviewers**

1、 K.M. Liew, Tel: (+852) 3442 6581; Fax: (+852) 2788 7612;E-Mail: kmliew@cityu.edu.hk

2、 J.Cai, Tel: +65-687-44328; fax:+65-677-63604; E-Mail: mascaij@nus.edu.sg

3、 F.G. Yuan, Tel:+1-919-515-5947; fax: +1-919-515-5934; E-Mail: yuan@eos.ncsu.edu

**Figure 1**

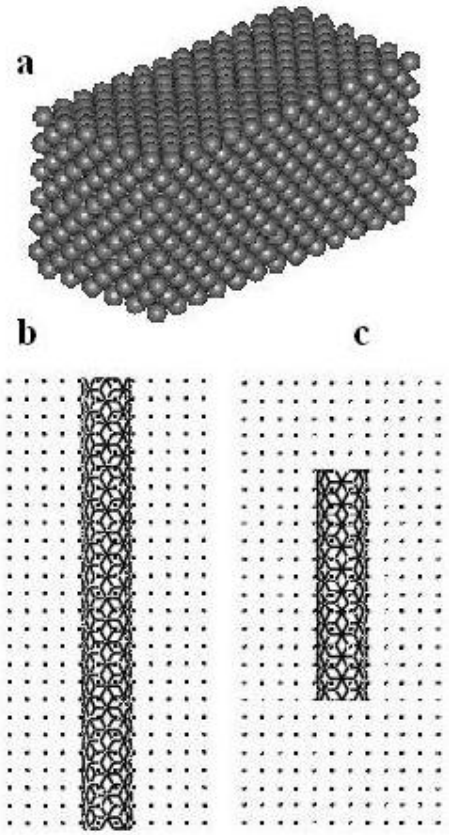

**Figure 2**

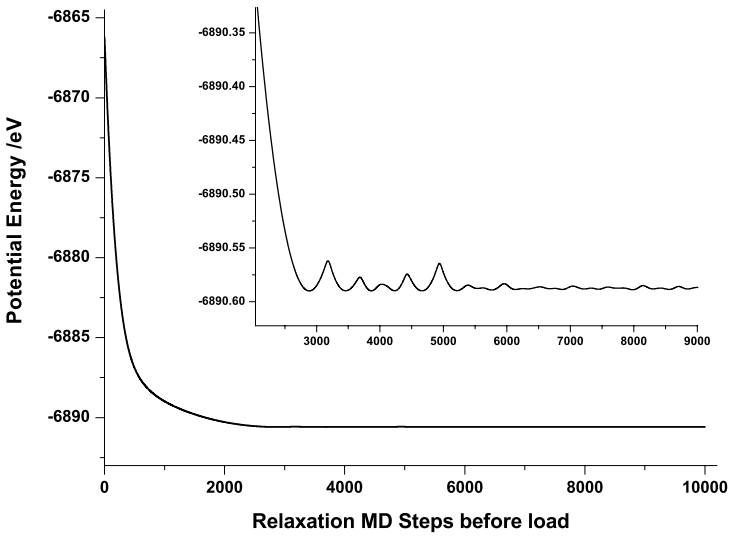
-6865
-6870
-6875
-6880
-6885
-6890
Potential Energy /eV
0
2000
4000
6000
8000
10000
Relaxation MD Steps before load
-6890.35
-6890.40
-6890.45
-6890.50
-6890.55
-6890.60
3000
4000
5000
6000
7000
8000
9000

**Figure 3**

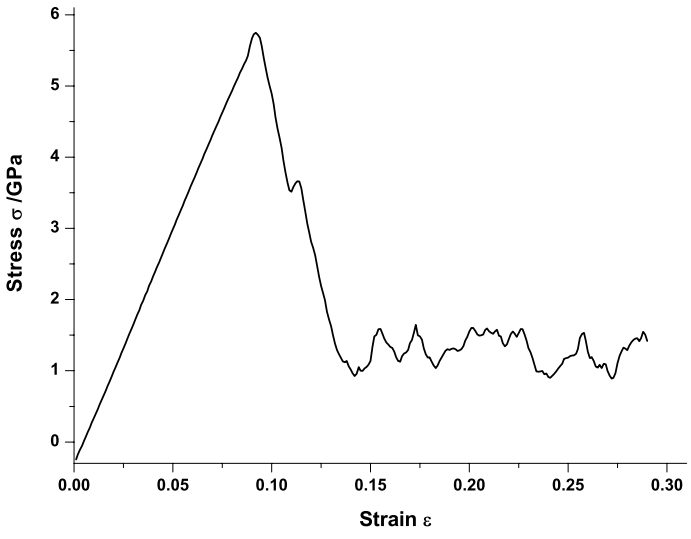

**Figure 4**

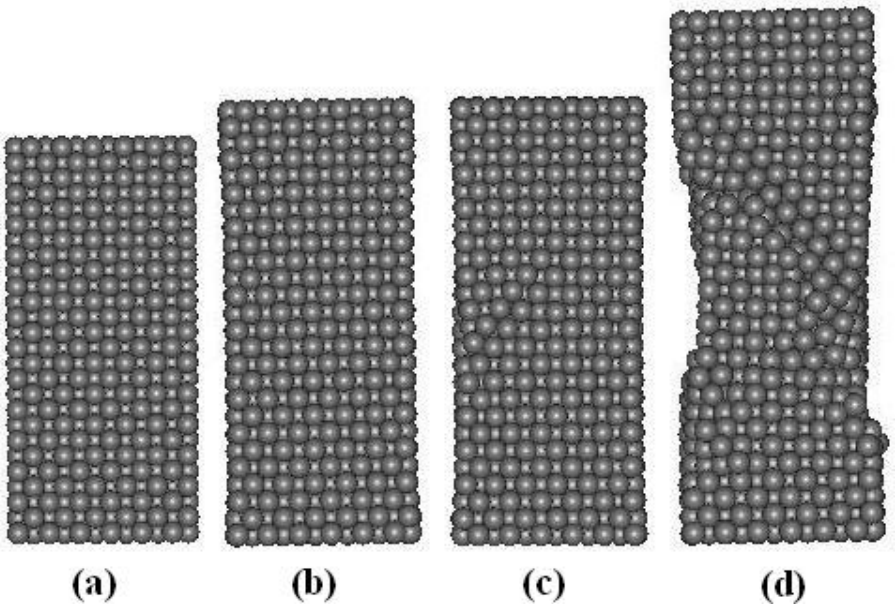

**Figure 5**

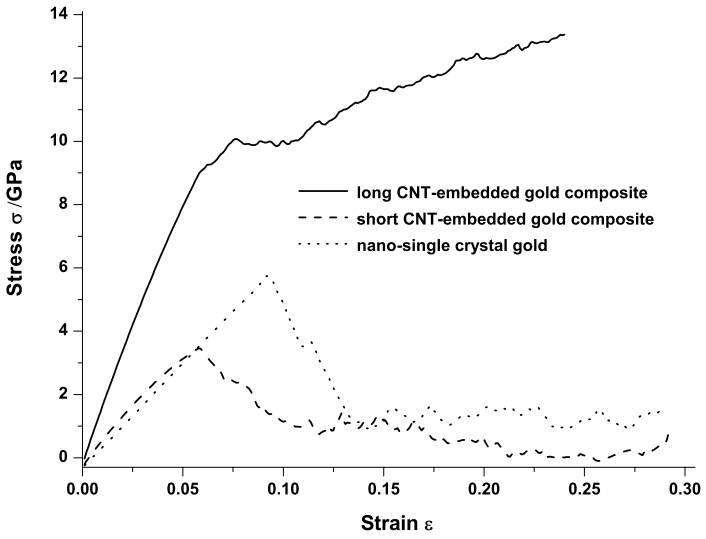
Stress σ /GPa
Strain ε
0
2
4
6
8
10
12
14
0.00
0.05
0.10
0.15
0.20
0.25
0.30
long CNT-embedded gold composite
short CNT-embedded gold composite
nano-single crystal gold

**Figure 6**